Generalized Processing for Pulsed Synthetic Aperture Radar

Evan C. Zaugg - zaugg@ee.byu.edu
Brigham Young University - Department of Electrical and Computer Engineering

***Abstract*—The Range-Doppler Algorithm (RDA) and the Chirp-Scaling Algorithm (CSA) process Synthetic Aperture Radar (SAR) data with approximations to ideal SAR processing. These approximations are invalid for data from systems with wide beamwidths, large bandwidths, and/or low center frequencies. While simple and efficient, these frequency-domain methods are thus limited by the SAR parameters. This paper explores these limits and proposes a generalized chirp-scaling approach for extending the utility of frequency-domain processing.**

We demonstrate how different order approximations of the SAR signal in the two-dimensional frequency domain affect image focusing for varying SAR parameters. From these results, a guideline is set forth which suggests the required order of approximation terms for proper focusing. A proposed generalized frequency-domain processing approach is derived. This method is an efficient arbitrary-order chirp-scaling algorithm that processes the data using the appropriate number of approximation terms. The new method is demonstrated using simulated data.

I. Introduction

NEW synthetic aperture radar systems operating with wide bandwidths at low frequencies [1]–[4] attract attention due to the potential for improving the data quality of existing applications and investigating new uses [5]–[10]. At low frequencies the approximations made in formulating a number of SAR processing algorithms, such as the Range-Doppler Algorithm (RDA) and the Chirp Scaling Algorithm (CSA), are no longer valid [11], [12]. Some of the errors caused by many of these approximations have been addressed, together with suggested remedies, in previous work [13]–[18]. Also at low frequencies, the wider beamwidth required for high azimuth resolution causes problems with the center beam approximation used in motion compensation [18], [19] and in the chirp scaling process used in the CSA [20].

Processing for low frequency SAR has typically been approached with inversion methods such as the Fourier-Hankel [21] and the wavenumber domain Omega-K (ω-k) [22]–[24] algorithm or time-domain processing methods [25]–[27]. These methods avoid the approximations that make RDA and CSA problematic at low frequencies and wide beamwidths, but unfortunately, they are more complex and computationally burdensome. The ω-k processing requires a costly interpolation to perform the Stolt mapping, and the algorithm makes it difficult to implement range-dependent motion compensation. Time-domain methods can be very precise for all SAR configurations, but are even more inefficient. Specialized hardware, such as graphics processing units (GPUs), has been shown to accelerate time-domain SAR and tomographic SAR processing [28]. While efforts have been made to modify the CSA to efficiently handle the effects of wide aperture [18], to extend the ω-k algorithm to handle range-dependent motion compensation [22], [29], [30], and to streamline the time-domain methods [26], [27], the common frequency-domain methods (RDA and CSA) are still widely used, despite their limitations, because of their simplicity and processing efficiency. This paper explores the limits of valid processing for these frequency-domain methods and proposes a generalized chirp-scaling SAR processing algorithm that efficiently extends the utility of frequency-domain processing for SAR systems with wide beamwidths, large bandwidths, and low frequencies.

In Section II, the general SAR signal in the two-dimensional frequency domain is derived. In Section III, the approximations made to this signal are analyzed. For approximations of an arbitrary number of terms, an expression is derived for the phase error at any point in the frequency support band. Simulated data is used to analyze the effects that these phase errors have on image focusing with different order approximations and varying SAR parameters. Section IV provides a guideline for determining the number of terms in the approximation required for properly focusing the SAR image. Finally, a generalized chirp-scaling SAR processing algorithm is derived that includes the appropriate number of terms.

II. The General SAR Signal

For our analysis, we consider only the phase functions of the SAR signal, ignoring the initial phase. As in the development presented in [31], we can describe the phase of the demodulated baseband SAR signal as

$$\Phi_0 = -4\pi f_0 R(\eta)/c + \pi K_r(\tau - 2R(\eta)/c)^2 \qquad (1)$$

where f_0 is the carrier frequency. $R(\eta)$ is the range to a given target at slow time η. K_r is the range, or fast time, chirp rate and τ is fast time.

The first term describes the azimuth modulation: it consists of the phase left over after demodulation. It is purely a function of the carrier frequency and the changing range to a target. The second term in Eq. (1) is the transmit chirp delayed by the two-way travel time to the target. If we were to reduce the bandwidth to a single frequency, the second term would go to zero, but we would still have the same azimuth modulation.

The approximations made in many SAR processing algorithms are calculated in the wavenumber, or two-dimensional frequency domain. The derivation of the general SAR signal

in the wavenumber domain, as found in Appendix A, results in

$$\Phi_{1RA} = -\frac{4\pi R_0 f_0}{c}\sqrt{D^2(f_\eta) + \frac{2f_\tau}{f_0} + \frac{f_\tau^2}{f_0^2}} - \frac{\pi f_\tau^2}{K_r} \quad (2)$$

where

$$D(f_\eta) = \sqrt{1 - \frac{c^2 f_\eta^2}{4v^2 f_0^2}}, \quad (3)$$

R_0 is the range of closest approach, f_τ is range frequency, and f_η is azimuth frequency.

Eq. (2) is the phase of the SAR signal in the wavenumber domain. For a target at a given range R_{ref}, the target can be ideally focused with the reference function multiply

$$H_{RFM} = \frac{4\pi R_{ref} f_0}{c}\sqrt{D^2(f_\eta) + \frac{2f_\tau}{f_0} + \frac{f_\tau^2}{f_0^2}} + \frac{\pi f_\tau^2}{K_r} \quad (4)$$

This works regardless of squint, beamwidth, and chirp bandwidth.

III. SAR Approximations

The CSA and RDA make approximations to Eq. (2) which break down at low-frequencies, large beamwidths, and large bandwidths. The ω-k algorithm can be a good choice in these situations because it uses the exact representation of Eq. (2) and applies Eq. (4) for a reference range while Stolt interpolation corrects for other ranges. This precision comes at the cost of increased complexity and for precise Stolt interpolation, the processing time increases compared to the CSA and RDA. Also, the ability to apply range-dependent motion compensation is hindered with the ω-k algorithm [22], [30].

The CSA and RDA approximations are formed using a Taylor series approximation of Eq. (2). The square root term can be expanded as

$$\begin{aligned}\Upsilon(f_\tau) &= \sqrt{D^2(f_\eta) + \frac{2f_\tau}{f_0} + \frac{f_\tau^2}{f_0^2}} \quad (5)\\ &\approx \Upsilon(0) + \frac{\Upsilon'(0)}{1!}f_\tau + \frac{\Upsilon''(0)}{2!}f_\tau^2 + \frac{\Upsilon'''(0)}{3!}f_\tau^3 \dots\end{aligned}$$

RDA keeps only the 0th order term

$$\Phi_{RDA} \approx -\frac{4\pi R_0 f_0}{c}\cdot[D(f_\eta)] - \frac{\pi f_\tau^2}{K_r} \quad (6)$$

which makes the algorithm relatively simple. The first term of Eq. (6) is the azimuth modulation, corrected in the range-Doppler domain during azimuth compression. The second term is the chirp modulation corrected in the range compression step. Range-cell migration (RCM) correction is an interpolation that makes up for the neglected first order RCM term while the secondary range compression potentially compensates for neglected higher order terms.

The CSA keeps up to the second order term [31], [32]

$$\begin{aligned}\Phi_{CSA} &\approx -\pi f_\tau^2/K_r - 4\pi R_0 f_0/c \cdot \\ &\quad \left[D(f_\eta) + \frac{f_\tau}{f_0 D(f_\eta)} + \frac{D^2(f_\eta)-1}{2f_0^2 D^3(f_\eta)}f_\tau^2\right] \quad (7)\end{aligned}$$

as shown inside the square brackets; the first term is the azimuth modulation, the second term is the range-cell migration, and the third term is cross-coupling between the range and azimuth frequencies. Important variations of the CSA have been introduced to address the limitations of this approximation. In the extended CSA of [13], a third-order chirp-scaling term is introduced for high squint with integrated motion compensation. Then in [14], the non-linear chirp-scaling algorithm is derived which includes a third-order SAR signal model, phase filter, and chirp-scaling parameter. The latter two are carefully chosen such that the range-dependence of the range-cell-migration (RCM) and secondary-range-compression (SRC) is eliminated. Another modification to the extended CSA in [15] is the inclusion of a range-scaling term which controls the bandwidth increase associated with chirp-scaling. Finally the quartic-phase algorithm [16] extends these concepts including a fourth-order phase filter and chirp-scaling parameter, a range-scaling term, and an improved model of range-dependence for SRC

These algorithms are based on specific order approximations, but more generally, we can expand Eq. (5) to an arbitrary number of terms:

$$\begin{aligned}\Upsilon(f_\tau) \approx\ & D(f_\eta) + \frac{f_\tau}{f_0 D(f_\eta)} + \frac{D^2(f_\eta)-1}{2f_0^2 D^3(f_\eta)}f_\tau^2 \quad (8)\\ & - \frac{D^2(f_\eta)-1}{2f_0^3 D^5(f_\eta)}f_\tau^3 - \frac{5-6D^2(f_\eta)+D^4(f_\eta)}{8f_0^4 D^7(f_\eta)}f_\tau^4\\ & + \frac{7-10D^2(f_\eta)+3D^4(f_\eta)}{8f_0^5 D^9(f_\eta)}f_\tau^5\\ & + \frac{-21+35D^2(f_\eta)-15D^4(f_\eta)+D^6(f_\eta)}{16f_0^6 D^{11}(f_\eta)}f_\tau^6\\ & - \frac{-33+63D^2(f_\eta)-35D^4(f_\eta)+5D^6(f_\eta)}{16f_0^7 D^{13}(f_\eta)}f_\tau^7 \dots\end{aligned}$$

The phase error due to this approximation can be expressed as

$$\begin{aligned}\Phi_{Error} &= \Phi_{1RA} + \frac{\pi f_\tau^2}{K_r} + \frac{4\pi R_0 f_0}{c}\cdot\Upsilon(f_\tau) \quad (9)\\ &= -\frac{4\pi R_0 f_0}{c}\cdot\left(\sqrt{D^2(f_\eta) + \frac{2f_\tau}{f_0} + \frac{f_\tau^2}{f_0^2}} - \Upsilon(f_\tau)\right)\end{aligned}$$

which is a function of four parameters:

1) range to target, R_0
2) center frequency, f_0
3) range frequency, f_τ, and
4) azimuth frequency, f_η.

The phase error gets larger when the range increases, the center frequency decreases, the maximum range frequency increases, and/or the maximum azimuth frequency increases.

The limits of f_τ are determined by the chirp bandwidth. For a chirp centered at zero after demodulation, the maximum and minimum f_τ are plus and minus half the bandwidth. For a chirp starting at zero, the maximum f_τ is the bandwidth. Thus as the bandwidth increases, the maximum f_τ increases. A larger f_τ means a larger approximation phase error in Eq. 9.

The maximum and minimum azimuth frequencies are a function of the beamwidth θ and squint ϑ

$$f_{\eta MAX} = 2\frac{f_0}{c}v\sin\left(\frac{\theta}{2}+\vartheta\right) \quad (10)$$

$$f_{\eta MIN} = 2\frac{f_0}{c}v\sin\left(-\frac{\theta}{2}+\vartheta\right). \quad (11)$$

f_η is only used in Eq. 9 as part of $D(f_\eta)$, which can be rewritten at maximum f_η as

$$D(f_{\eta MAX}) = \sqrt{1-\sin^2\left(\frac{\theta}{2}+\vartheta\right)}, \quad (12)$$

thus the azimuth frequency dependence of the phase error in Eq. 9 is dependent on the beamwidth and independent of velocity and PRF.

Simulated data are used to demonstrate how changing the radar parameters affects the azimuth focusing. A nominal choice of SAR parameters is chosen, with images created with no approximations and with the CSA approximations. The four paramters that affect the phase error are individually varied to demonstrate how the focusing changes with these parameters. The initial radar parameters are a center frequency of 1.75 GHz, a bandwidth of 500 MHz centered at zero, an altitude of 3050 meters, and a beamwidth 19.3° wide. An image of a single point target, ideally processed using Eq. 2 without approximations (ω-k algorithm), is shown in Fig. 1. The same data processed with the CSA (second order approximation) is shown in Fig. 2.

The CSA was used in producing Figs. 3-6, which show the results of changing, respectively, the range to target, the center frequency, the chirp bandwidth, and the antenna beamwidth. The azimuth resolution changes with center frequency and beamwidth, Fig. 7 shows two examples of changing the beamwidth and center frequency to keep the along-track resolution the same. The results from these figures are summarized in Table I.

IV. SAR Processing Generalization

For any given set of SAR system parameters, a generalized frequency-domain SAR processor must:

1) Determine the number of terms (order) from Eq. (8) that is required for proper focusing
2) Efficiently process the data taking into account those terms.

A. Required Order Determination

One approach to accomplishing the first step is by considering the phase error from Eq. (9). This error can be viewed and analyzed by computing the error for every point in the support band in the two-dimensional frequency domain. Phase errors greater than a few tenths of a radian indicate that a portion of the data is being processed incorrectly. We choose a threshold of $\pi/10$ to be excess error. The portion of the support band with phase errors greater than $\pi/10$ can be used to predict the focusing accuracy of a target. This percentage is calculated for each example in Table I and the results are shown in Fig. 8. From this graph we devide on a guideline: if less than 30% of the support band has a phase error greater than $\pi/10$, then one can predict less than a 20% loss in azimuth resolution defocusing. Depending on error tolerances of a given application, 20% loss of focus could be inadequate. In that case, processing the data with more of the higher order terms from Eq. (8) is advised.

If the third-order terms are included in processing the data from Fig. 2, the percentage of phase errors greater than $\pi/10$ drops to 10.6% and the focusing is indistinguishable from the the ideal (1.9% defocus), as shown in Fig. 9. Dropping the frequency to 1.25 GHz and increasing the beamwidth to 27.1° maintains the theoretic azimuth resolution of 22.6 cm, but the percentage of phase errors greater than $\pi/10$ increases to 31.2%, and Fig. 10 shows that the focusing decreases by 16.7%, which is expected based on the guidelines of Fig. 8.

As another example, data is simulated with a center frequency of 800 MHz, a bandwidth of 500 MHz, a beamwidth of 40.3°, and range to target 1755.6 m. The data is repeatedly processed with terms of increasing order. The results are shown in Fig. 13 and summarized in Table II. Again we find that the defocusing is reduced to about 20% as the percent of phase error greater than $\pi/10$ drops to about 30%.

The above guidelines suggest the order of the terms required for proper focusing. Efforts have been made to develop algorithms for efficiently processing data while keeping the higher order terms. As an example, from the algorithms mentioned in Section III, the non-linear CSA algorithm of [14] keeps up to the 3rd order term of Eq. (8). Compared to the CSA, this method requires two additional range FFT's and a phase multiply. If terms higher than the 3rd order are needed for proper focusing, something more involved than the non-linear CSA is required. Such a method is derived below.

There is an upper bound for the number of approximation terms that can be used. An extreme situation is simulated with a center frequency of 350 MHz, a bandwidth of 500 MHz, an antenna beamwidth of 80°, and a range to target of 3003 m. Fig. 11 shows that the highest order approximation that yields the best results is the 6th order. Using terms higher than this are actually detrimental to the overall focusing. As seen in Fig. 12 and in Eq. (8), the higher order terms become increasingly important at the edges of the support band. The terms come in alternating positive and negative pairs which largely cancel each other out, and above the 6th order the terms are too unstable for practical use. With this particular set of parameters, however, even when using the 6th order approximation, 61.6% of the support band has a phase error greater than $\pi/10$. Thus a frequency domain processing method is inadequate for focusing this data. This result suggests that there is a definite point at which SAR processing *requires* an ω-k or time-domain approach, in such cases, a frequency-domain approach should not be used.

B. Generalized SAR Processing Algorithm

The goal is to develop a new general processing scheme which efficiently accounts for as many higher order terms as dictated by the SAR parameters and the desired precision. Ideally, each additional term from Eq. (8) should add minimally

TABLE I

SUMMARY OF THE SIMULATION PROCESSING PARAMETERS AND RESULTS FOR FIGS. 1-7. THE "DEFOCUS FACTOR" IS THE PERCENT INCREASE IN MEASURED AZIMUTH RESOLUTION OVER THE THEORETICAL AZIMUTH RESOLUTION. THE THEORETICAL AZIMUTH RESOLUTION FOR AN UNWEIGHTED APERTURE IS $(0.89 \cdot c/(4f_0 sin(\theta/2))$.

	Range to Target (m)	Center Frequency (GHz)	Chirp Bandwidth (MHz)	Antenna Beamwidth (°)	Theoretical Azimuth Resolution (m)	Measured Azimuth (m) Resolution (m)	Defocus Factor (%)	Percent of Phase Error Greater Than $\pi/10$ (%)
Fig. 1	3053.2	1.75	500	19.3	22.6	22.6	0.0	0.0
Fig. 2	3053.2	1.75	500	19.3	22.6	29.0	28.1	41.0
Fig. 3	1531.4	1.75	500	19.3	22.6	24.5	8.3	31.2
	6101.6	1.75	500	19.3	22.6	32.0	41.5	50.1
Fig. 4	3053.2	1.5	500	19.3	26.4	33.9	28.5	45.2
	3053.2	2	500	19.3	19.8	31.9	41.1	37.3
Fig. 5	3053.2	1.75	250	19.3	22.6	23.7	4.6	11.4
	3053.2	1.75	500	19.3	22.6	31.2	37.9	67.0
Fig. 6	3053.2	1.75	500	9.6	45.5	47.3	3.9	20.8
	3053.2	1.75	500	29.0	15.1	25.1469	66.4	51.7
Fig. 7	3053.2	1.5	500	22.5	22.6	30.6	35.4	49.2
	3053.2	2	500	16.9	22.6	27.6	22.1	33.4

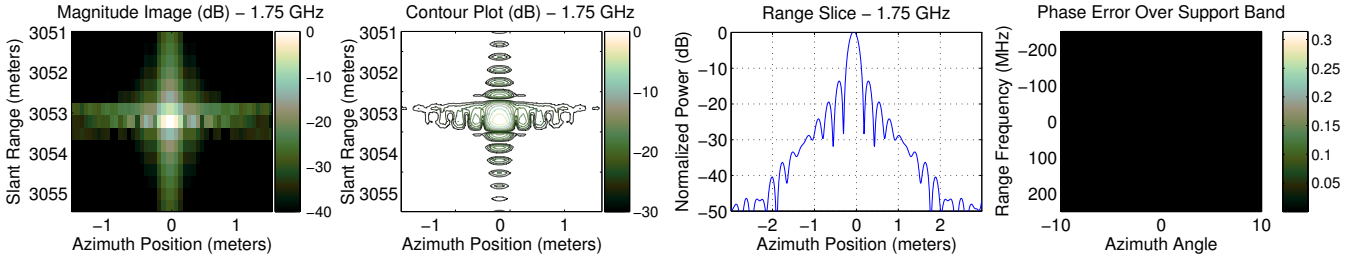

Fig. 1. Simulated SAR data of a single point target at a range of 3053.2 m, a center frequency of 1.75 GHz, a chirp bandwidth of 500 MHz and an antenna beamwidth of 19.3°, ideally processed without approximations (ω-k, Eq. (4)). The left-most plot is a magnitude image of the focused target. The next figure is a contour plot with contours spaced 3dB apart. The next plot is a range slice through the center of the target, plotted in dB, the azimuth resolution is measured at the 3 dB point of this figure. The right-most image shows the phase error over the support band due as in Eq. (9). The parameters and results for this data are summarized in Table I.

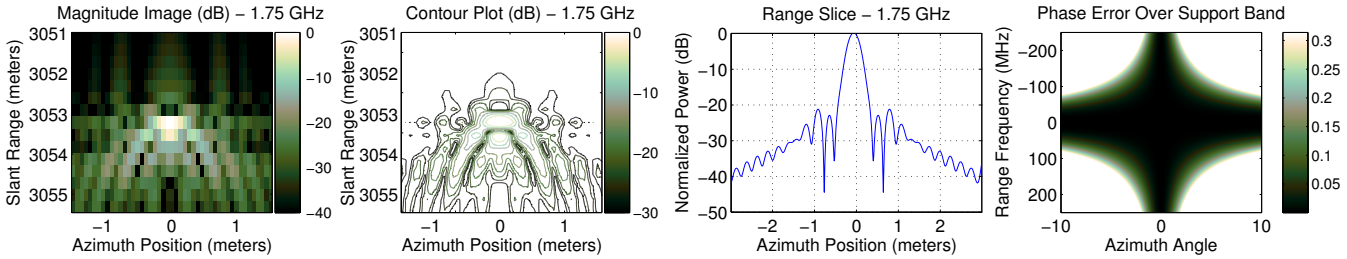

Fig. 2. Simulated SAR data of a single point target at a range of 3053.2 m, a center frequency of 1.75 GHz, a chirp bandwidth of 500 MHz and an antenna beamwidth of 19.3°, processed using the CSA (2nd order approximation). The plots are arranged as in Fig. 1. Parameters and results are summarized in Table I.

to the computational burden. The algorithm derived below is summarized in Table III. For order n, the high-order phase and chirp-scaling terms up to the n_{th} order are chosen such that the range dependence of the range-cell migration and range-frequency rate is removed.

We start with the approximation of the phase of our signal in the two-dimensional frequency domain, Eq. (2), which we express as Φ_{SS} in row 4 of Table III, where Υ_i is the ith derivative of $\Upsilon(f_\tau)$ evaluated at $f_\tau = 0$, as in Eq. (5).

This signal is multiplied by a higher-order phase filter, H_{HOPF} in row 5 of Table III. The X_i terms are solved later in the derivation to remove the range-dependence of the higher order terms.

The inverse range Fourier transform is approximated by the principle of stationary phase (POSP). Assuming the higher-order terms are small, as in [14], [16], [33], the signal in the range-Doppler domain can be shown to be Φ_{sSm} in row 6 of Table III, where, as in [14], [31],

$$K_m = \frac{Kr}{1 - \frac{K_r c R_0 f_\eta^2}{2v^2 f_0^3 D^3(f_\eta)}} \tag{13}$$

and $\tau_d = (2R_0)/(cD(f_\eta))$. τ_d is the trajectory of a target with

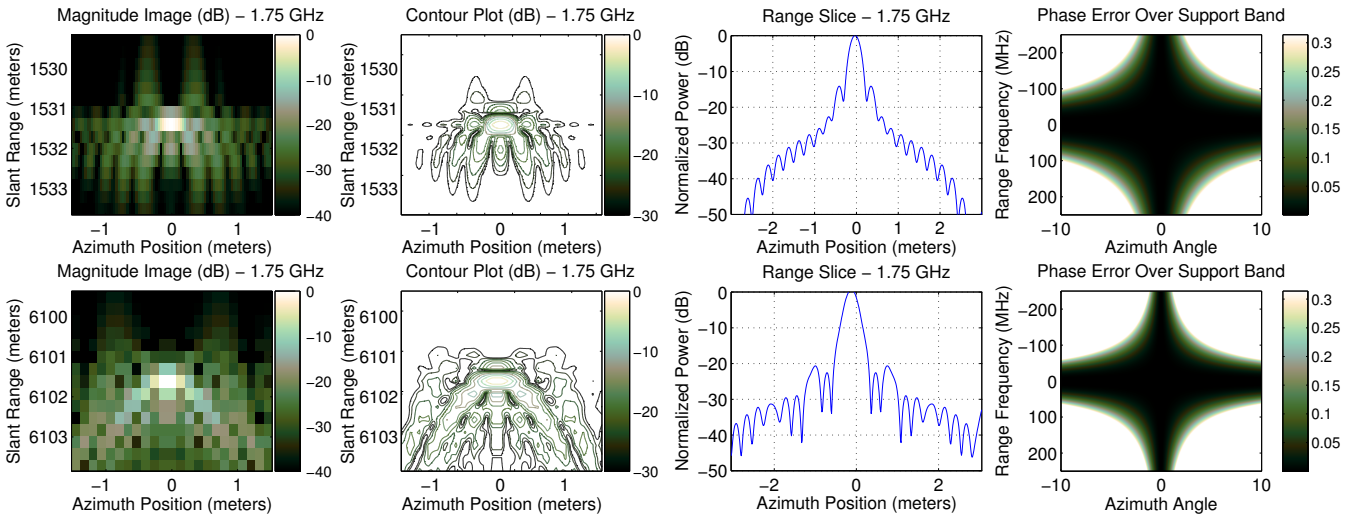

Fig. 3. Simulated SAR data of a single point target at ranges of 1531.4 m (top) and 6101.6 m (bottom), a center frequency of 1.75 GHz, a chirp bandwidth of 500 MHz and an antenna beamwidth of 19.3°, processed using the CSA. The plots are ordered as in Fig. 1. Compared to Fig. 2, the measured azimuth resolution improves at shorter range and worsens at longer range.

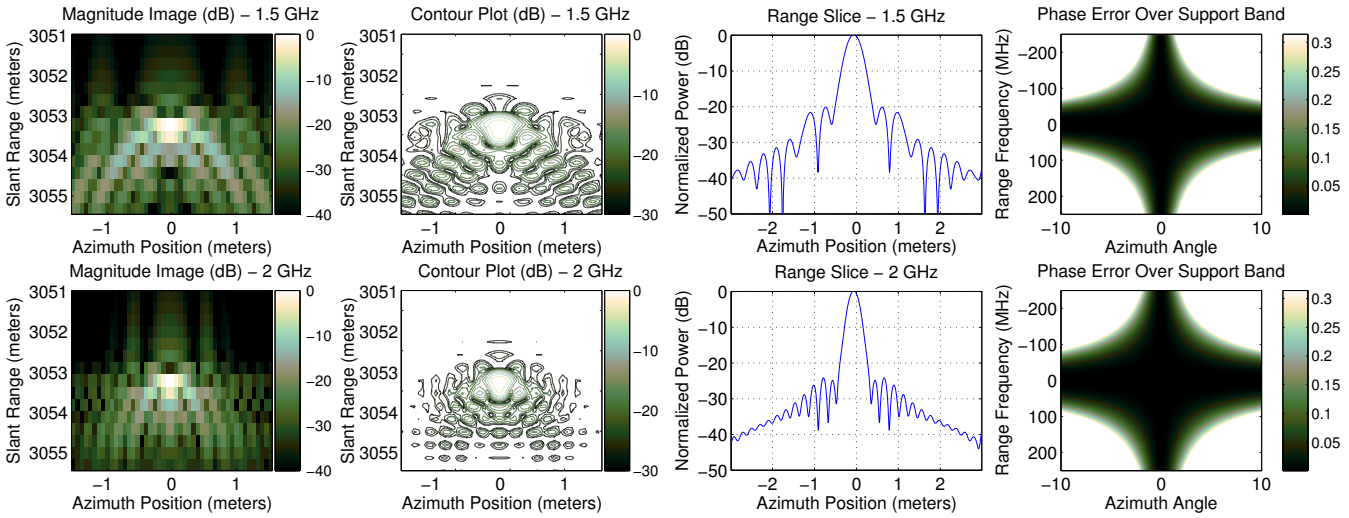

Fig. 4. Simulated SAR data of a single point target at a range of 3053.2 m, a center frequency of 1.5 GHz (top) and 2.0 GHz (bottom), a chirp bandwidth of 500 MHz and an antenna beamwidth of 19.3°, processed using the CSA. The plots are arranged as in Fig. 1. Compared to Fig. 2, the different center frequencies cause a change in the theoretical azimuth resolution, with the higher frequency focusing more accurately.

range of closest approach R_0.

The chirp-scaling is performed by a phase multiply of orders up through n. The chirp-scaling phase is H_{CS} in row 7 of Table III, where the q_i's are the scaling coefficients, which we will solve for, and $\tau_{ref} = (2R_{ref})/(cD(f_\eta))$, which is the trajectory for a target at reference range R_{ref}.

After chirp-scaling the signal phase is Φ_{sSz} in row 8 of Table III, where the first term is the along-track modulation, which we will ignore for the moment. The remaining terms, shown as the sum of C_i, are formed by making the substitutions

$$\tau_{ref} = \tau_s - \alpha\Delta\tau \tag{14}$$

$$\tau_d = \tau_s - (\alpha - 1)\,\Delta\tau \tag{15}$$

where $\Delta\tau = (2(R_0 - R_{ref}))/(cD(f_\eta))$, the difference between τ_d and τ_{ref}, and α is a scaling term determined by the Doppler centroid, f_{dc},

$$\alpha(f_\eta) = \frac{\sqrt{1 - \frac{c^2 f_\eta^2}{4v^2 f_0^2}}}{\sqrt{1 - \frac{c^2 f_{dc}^2}{4v^2 f_0^2}}} \tag{16}$$

which simplifies to $D(f_\eta)$ when there is no squint. Carefully expanding the result, and reordering the terms as a series of $(\tau - \tau_s)$ yields

$$C_0 + C_1\,(\tau - \tau_s) + C_2\,(\tau - \tau_s)^2 \ldots C_n\,(\tau - \tau_s)^n \tag{17}$$

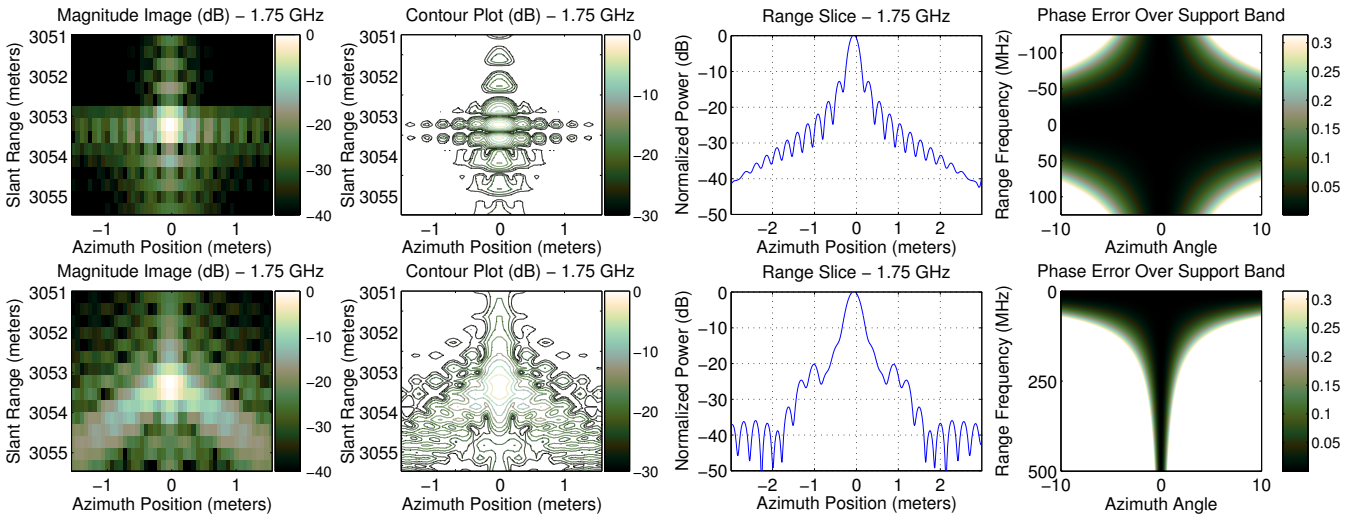

Fig. 5. Simulated SAR data of a single point target at a range of 3053.2 m, a center frequency of 1.75 GHz, a chirp bandwidth of 250 MHz centered at zero (top) and 500 MHz centered at 250 MHz (bottom), and an antenna beamwidth of 19.3°, processed using the CSA. The plots are arranged as in Fig. 1. Compared to Fig. 2, the top figure shows an improvement in azimuth focusing with a loss in range resolution while the bottom image shows degraded azimuth focusing.

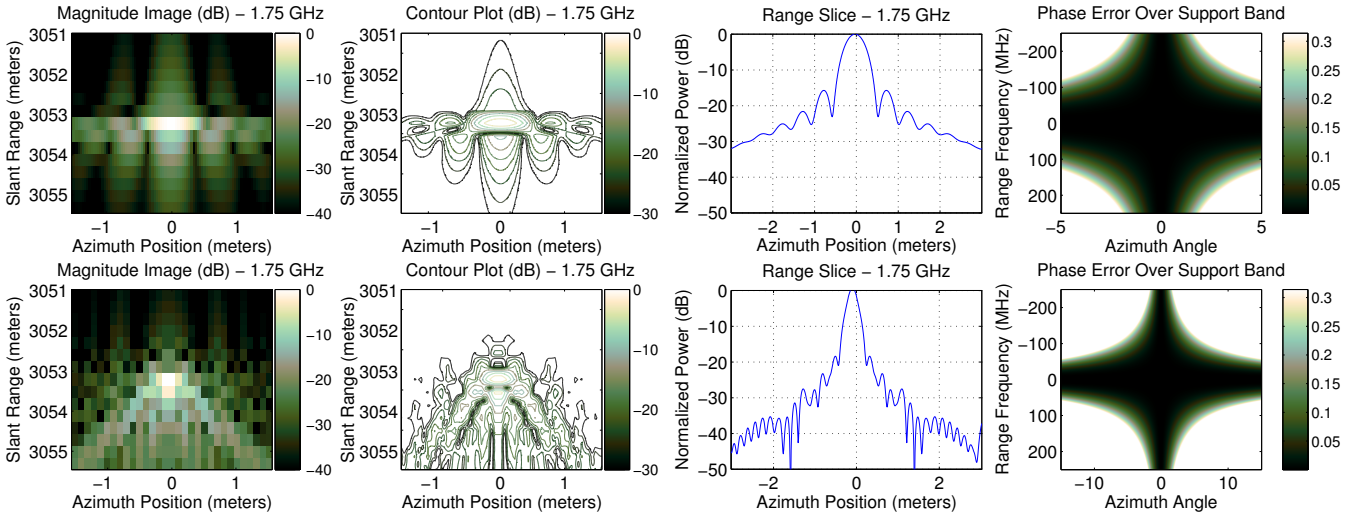

Fig. 6. Simulated SAR data of a single point target at a range of 3053.2 m, a center frequency of 1.75 GHz, a chirp bandwidth of 500 MHz and an antenna beamwidth of 9.6° (top) and 29.0° (bottom), processed using the CSA. The plots are arranged as in Fig. 1. Compared to Fig. 2, the changing beamwidths cause a change in the theoretical azimuth resolution.

where C_i is defined as

$$\begin{aligned} C_0 &= C_{x0} + \pi K_m \Delta\tau^2 (\alpha - 1)^2 \\ C_1 &= C_{x1} + 2\pi K_m (\alpha - 1) \Delta\tau \\ C_2 &= C_{x2} + \pi K_m \\ C_i &= C_{xi} \quad \text{for i} > 2 \end{aligned} \tag{18}$$

with

$$C_{xi} = \sum_{h=i}^{n} \left(\frac{h!}{i!(h-i)!} \pi (\alpha \Delta\tau)^{(h-i)} q_h \right) + \sum_{h=i}^{n} \left(\frac{2\pi K_m^i (\Delta\tau(\alpha-1))^{h-i} \left(\frac{f_0 \Upsilon_h \left(2R_{ref} + \Delta\tau D(f_\eta) c\right)}{c} - \frac{h! X_h}{2} \right)}{i!(h-i)!} \right) \tag{19}$$

where $X_i = 0$ and $\Upsilon_i = 0$ for $i < 3$ and $q_i = 0$ for $i < 2$.

The range-dependent range frequency rate K_m is approximately expressed as the sum of K_f, which is K_m at a reference range, and $\Delta\tau$. We first define

$$K_s = -\frac{c^2 f_\eta^2}{4v^2 f_0^3 D^2(f_\eta)} \tag{20}$$

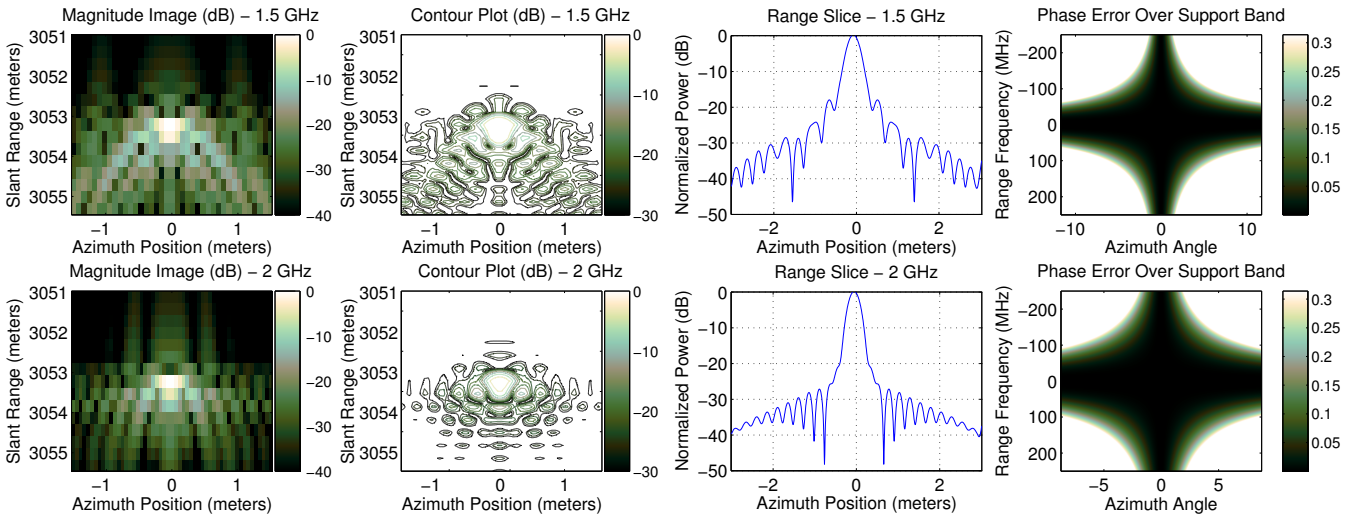

Fig. 7. Simulated SAR data of a single point target at a range of 3053.2 m, and a chirp bandwidth of 500 MHz, processed using the CSA. The plots are arranged as in Fig. 1. To maintain the same theoretical azimuth resolution as Fig. 2, the center frequency and antenna beamwidth are both changed in these figures. The top row has a lower frequency (1.5 GHz) and larger beamwidth (22.5°) while the bottom row has a higher frequency (2.0 GHz) and smaller beamwidth (16.9°), with results in Table I.

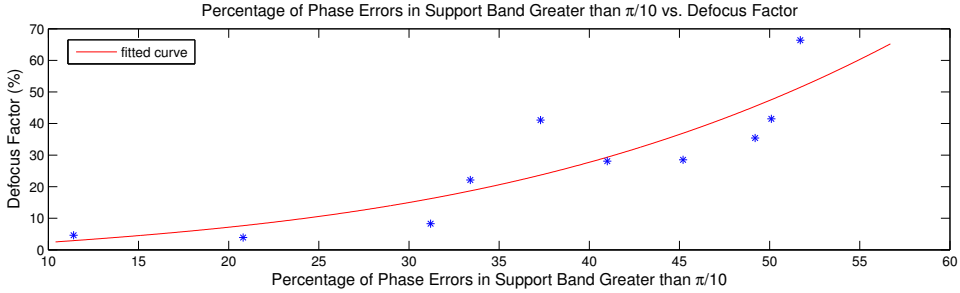

Fig. 8. From the data in Table I, the amount of defocusing is plotted versus the percentage of phase errors greater than $\pi/10$ in the support band. The general trend is emphasized with a fitted curve. From this we decide that in order to have less than a 20% loss in azimuth focus, the percentage of phase errors in the support band greater than $\pi/10$ should be less than 30%.

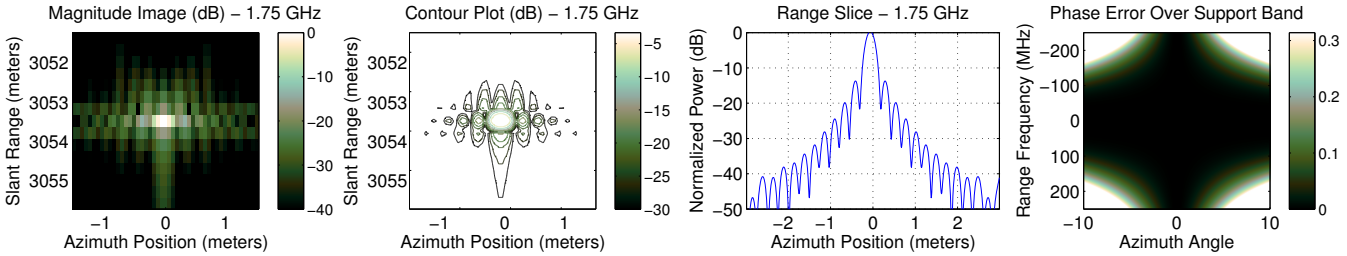

Fig. 9. Simulated SAR data of a single point target identical to Fig. 2, processed including third order approximation terms. The measured azimuth resolution is 23.0 cm, essentially equivalent to the theoretic value of 22.6 cm.

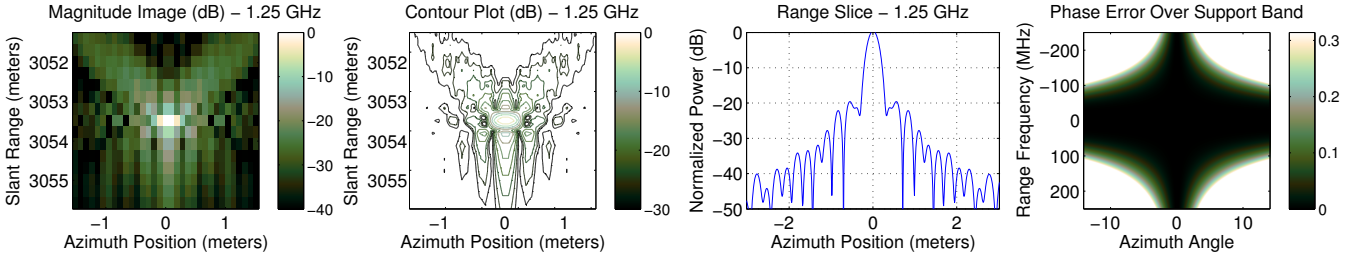

Fig. 10. Simulated SAR data of a single point target with a center frequency of 1.25 GHz, a beamwidth of 27.1°, and a 500 MHz bandwidth, processed with third-order approximations. The percent of the support band with a phase error greater than $\pi/10$ is 31.2%, this results in a measured azimuth resolution of 26.8 cm, a 16.7% loss of focus.

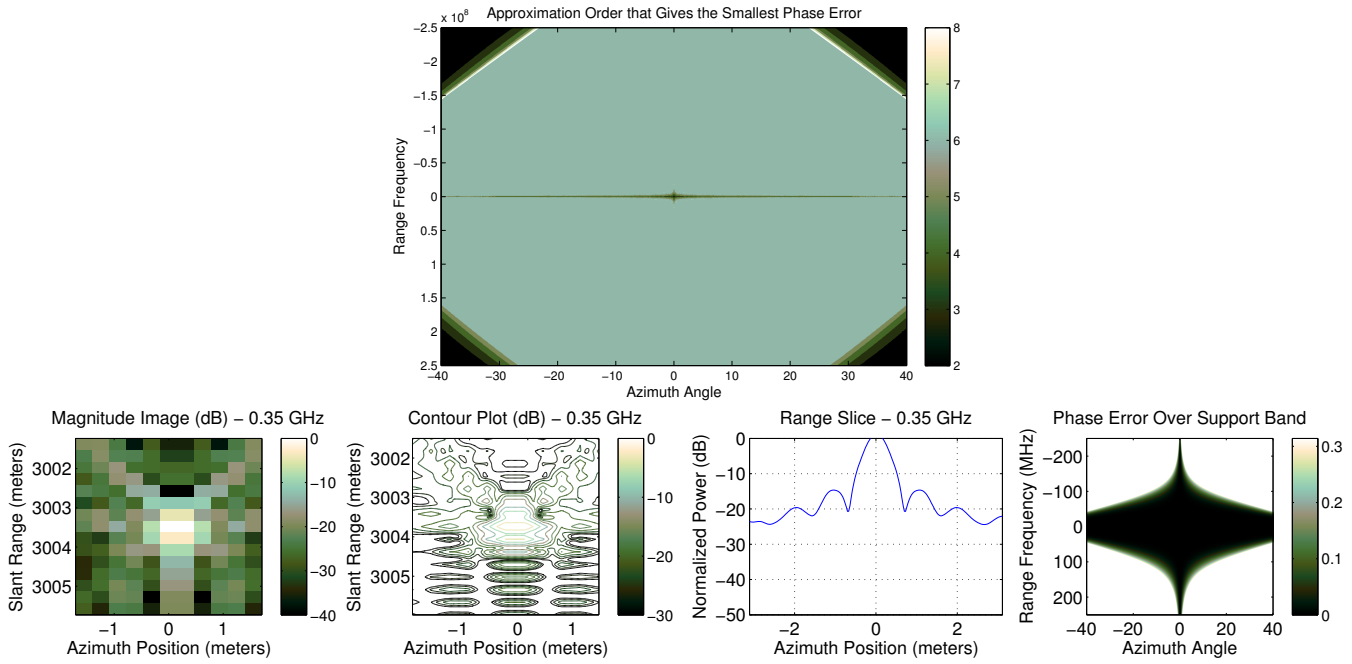

Fig. 11. In an extreme SAR situation, with a center frequency of 350 MHz, a 500 MHz bandwidth, a 80° beamwidth, and a 3003 m range to target, the top plot shows the approximation order closest to ideal over the support band, or the approximation order with the smallest error at each point over the support band. Interestingly enough, the sixth-order approximation is the best over the usable area of the support band with higher-order approximations performing worse. The SAR data is processed using the 6th order approximation, but even so, 61.6% of the support band has a phase error greater than $\pi/10$, and the measured azimuth resolution is 59.6 cm, a 101.5% defocus from the theoretic resolution of 29.6 cm.

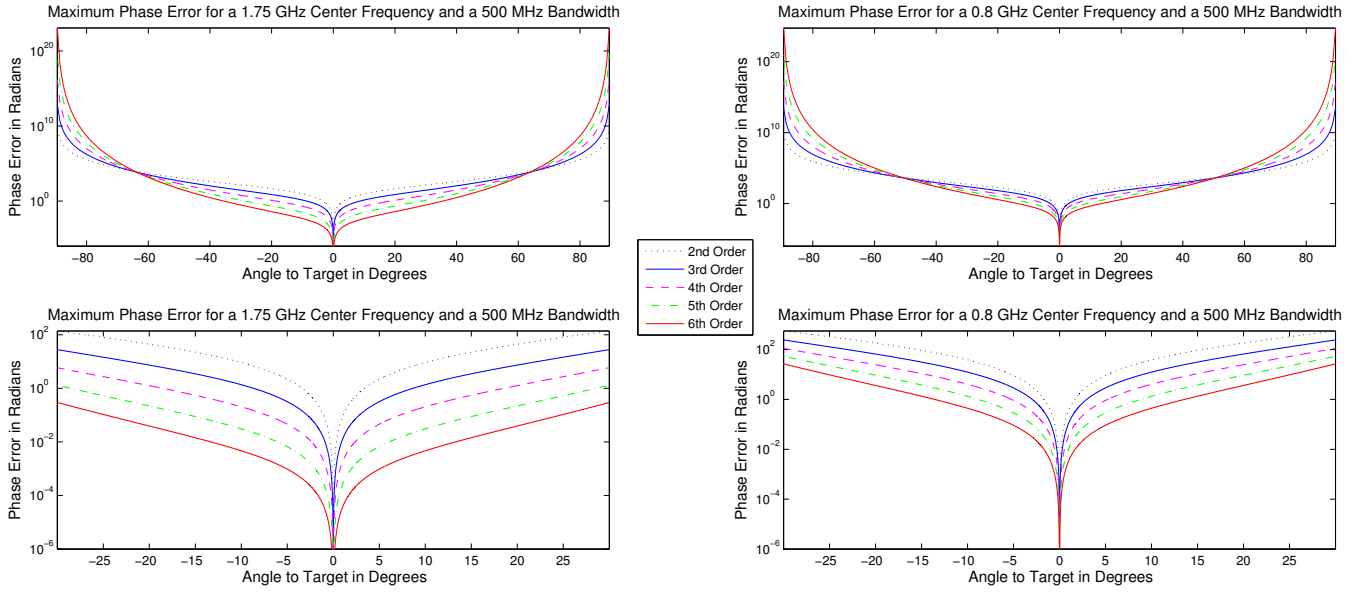

Fig. 12. The maximum magnitude of the phase error for different order approximations, as given by Eq. (9) for a 500 MHz bandwidth at 1.75 GHz (left) and 800 MHz (right). The top row shows the errors out to the maximum beamwidth of 180° while the bottom row focuses on beamwidths up to 60°. As the center frequency decreases, higher order approximations are required, even at small beamwidths, to get small phase errors. In addition, at lower frequencies a much larger beamwidth is required to maintain the same azimuth resolution, making it doubly important to account for the higher order terms. At extreme values, the higher order terms become dominate, marking the boundary of utility for frequency domain SAR processing.

then equivalent to Eq. (13)

$$K_m = -\frac{K_f}{-1 + K_s \Delta\tau K_f} \tag{21}$$

We Taylor expand K_m in terms of $\Delta\tau$, and keep up to the second order,

$$K_m \approx K_f + K_s K_f^2 \Delta\tau + K_s^2 K_f^3 \Delta\tau^2 \tag{22}$$

Each C_i for $i > 0$ is expressed as a series of $\Delta\tau$, for example

$$C_1 = 2\pi \left(\alpha K_f + q_2 \alpha - K_f\right) \Delta\tau \tag{23}$$

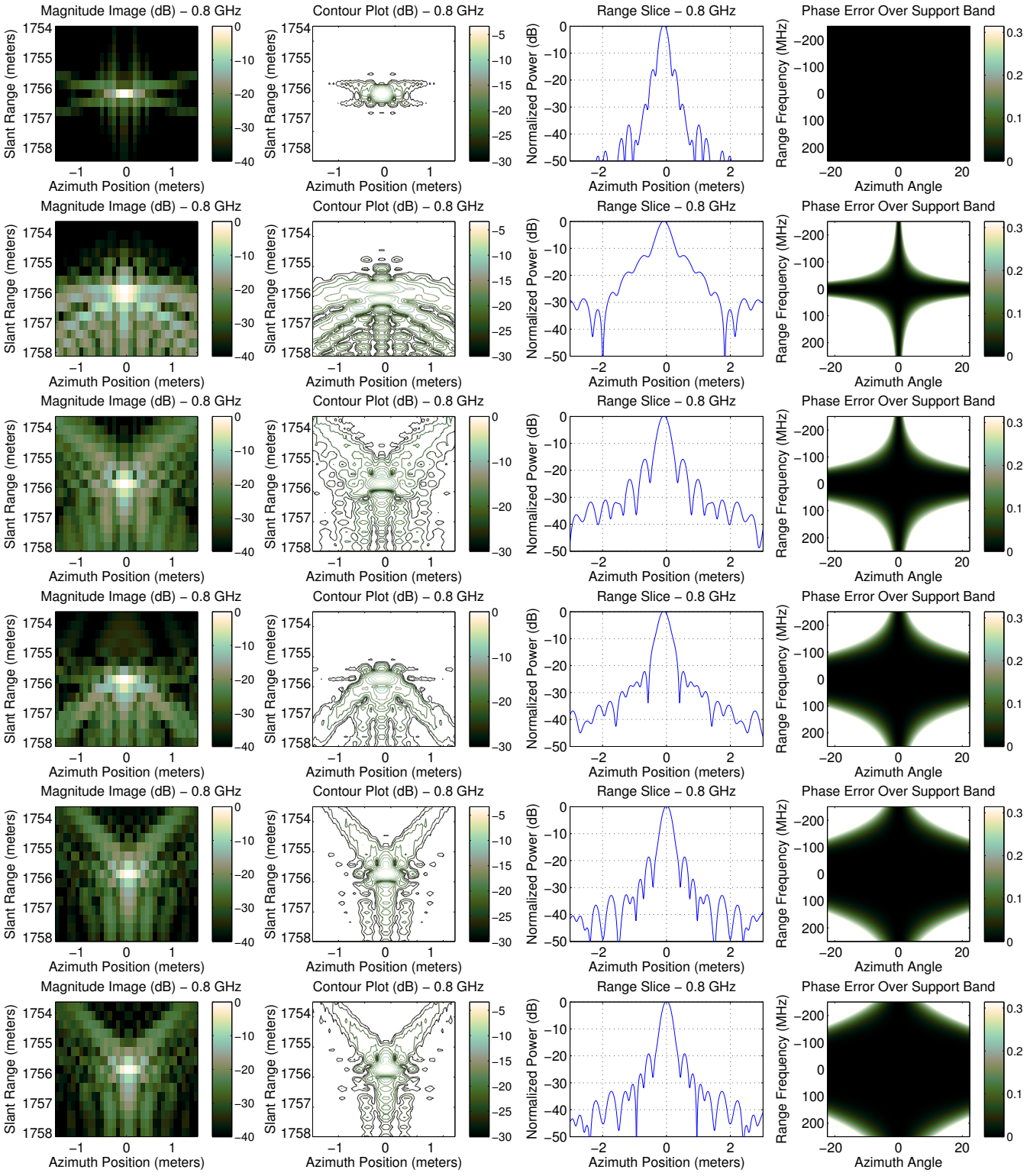

Fig. 13. Simulated SAR data of a point target at the reference range with a center frequency of 800 MHz, a bandwidth of 500 MHz, a beamwidth of 40.3°, and range to target 1755.6 m. Approximation orders two through six and ideal processing are used with results summarized in Table II. The top row shows ideal processing. Approximation orders two through six are shown in rows two through six respectively.

$$+\left(\frac{\pi K_f^3(\alpha-1)^2\left(2f_0\Upsilon_3 R_{ref}-3X_3c\right)}{c}+2\pi K_s K_f^2(\alpha-1)+3\pi q_3\alpha^2\right)\Delta\tau^2$$

$$+\ldots$$

When the coefficients of $\Delta\tau$ are zero, the range variations are eliminated. For the linear and quadratic terms of $\Delta\tau$, setting them equal to zero results in $2n-3$ equations for $2n-3$ unknowns, for example

$$2\pi(\alpha K_f+q_2\alpha-K_f)=0 \tag{24}$$

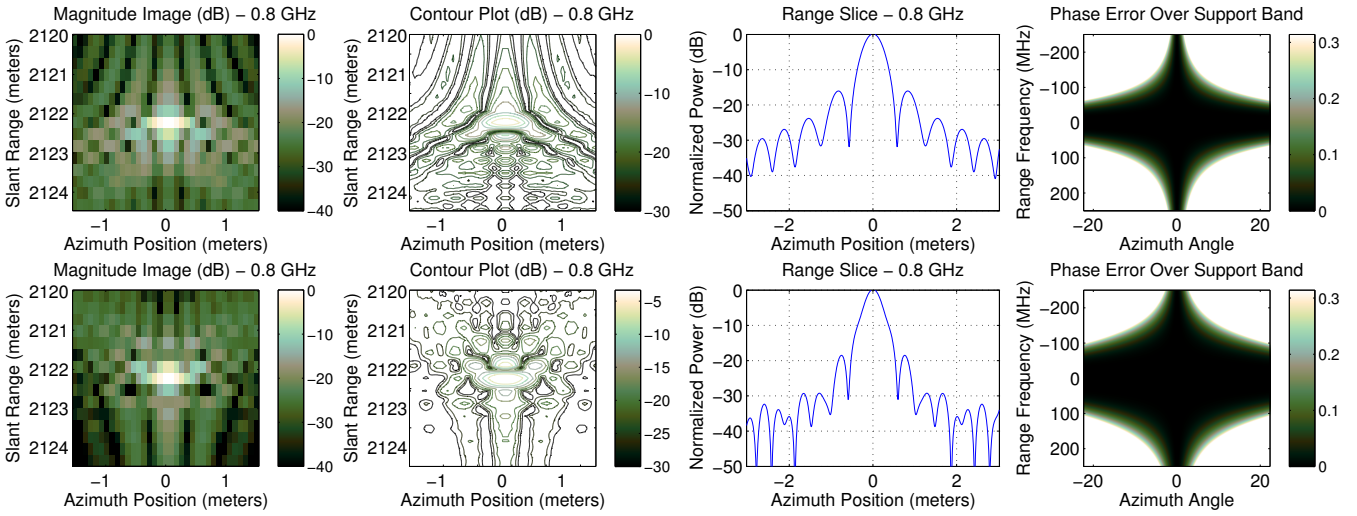

Fig. 14. The processed image of a second point target from the simulations of Fig. 13 more than 300 m away from the reference range. The top figure shows this target after 3rd order processing and the bottom figure shows the results of the 4th order processing. The generalized processing is designed to remove range dependence, demonstrated by the fact that the focusing of this target improves when processed with a higher-order approximation.

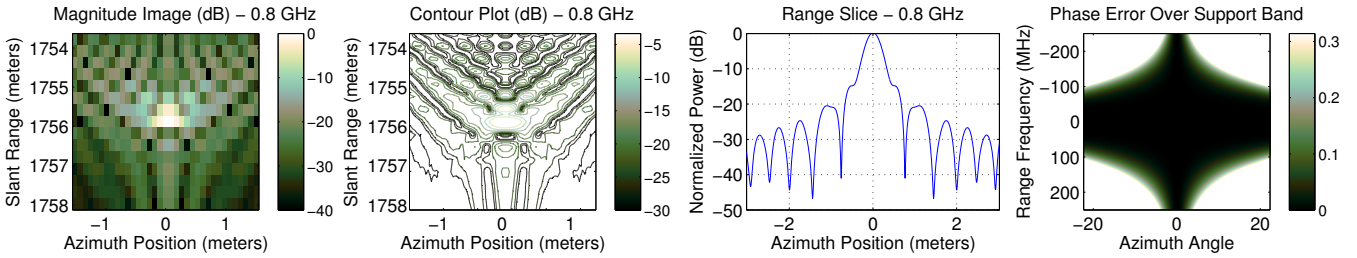

Fig. 15. The same data from Fig. 13 processed with an approximation to the generalized algorithm, shown here is the 4th order results. A processing time savings of 30% comes at the cost of higher sidelobes.

TABLE II
THE NUMERICAL RESULTS FROM THE IMAGES IN FIG. 13.

Approximation Order	Theoretic Azimuth Resolution (cm)	Measured Azimuth Resolution (cm)	Defocus Factor (%)	Percent of Phase Error Greater Than $\pi/10$ (%)	Processing Time as a multiple of CSA
2nd Order (CSA)	23.7	36.6	54.4	70.3	1
3rd Order	23.7	30.0	26.6	51.2	2.2
4th Order	23.7	29.1	22.7	33.9	3.6
5th Order	23.7	28.3	19.4	20.0	5.4
6th Order	23.7	27.7	16.8	10.1	7.2
Ideal	23.7	23.7	0.1	0.0	6.85

$$\frac{\pi K_f^3(\alpha-1)^2\left(2f_0\Upsilon_3 R_{ref}-3X_3c\right)}{c}+2\pi K_s K_f^2(\alpha-1)+3\pi q_3\alpha^2=0$$

$$\frac{\pi K_f^3(\alpha-1)\left(2f_0\Upsilon_3 R_{ref}-3X_3c\right)}{c}+\pi K_s K_f^2+3\pi q_3\alpha=0$$

$$etc.$$

We solve for q_i and X_i in Table IV

The linear and quadratic terms of $\Delta\tau$ in each C_i for $i>0$ become zero, while the higher order terms are very small and can be neglected. This results in the SAR signal phase being expressed as in the second part of row 8 of Table III.

A range FFT takes the signal into the two-dimensional frequency domain, resulting in Φ_{SS2} in row 9 of Table III. The signal is multiplied by a range matched filter, H_R in row 10 of Table III.

A range inverse Fourier transform is then calculated, resulting in a signal with a phase that is compensated by an azimuth compression and residual phase compensation H_{az} in Table III. An inverse azimuth Fourier transform results in the focused image.

This generalized method was applied in processing the data shown in Fig. 13 and Fig. 14. Significant improvements in focusing are seen, as detailed in Table II.

Of note is the relationship of this algorithm with those previously developed. When $n=2$, this algorithm simplifies to the CSA. When $n=3$, it simplifies to the non-linear CSA [14], without the extra orbital geometry term. If the α term is coupled with a β term that scales the range bandwidth, so that everywhere there is an α it becomes $\alpha\beta$, then when $n=2$

TABLE III
NTH-ORDER GENERALIZED CHIRP-SCALING PROCESSING FLOW

Action	Parameter Value
1. Digitize SAR Signal $\rightarrow e^{j\Phi_0}$	$\Phi_0 = -4\pi f_0 R(\eta)/c + \pi K_r(\tau - 2R(\eta)/c)^2$
2. Azimuth FFT	
3. Range FFT $\rightarrow e^{j\Phi_{1RA}}$	$\Phi_{1RA} = -\frac{4\pi R_0 f_0}{c}\sqrt{D^2(f_\eta) + \frac{2f_\tau}{f_0} + \frac{f_\tau^2}{f_0^2}} - \frac{\pi f_\tau^2}{K_r}$
4. Approximate Φ_{1RA} as Φ_{SS}	$\Phi_{SS} = -\pi f_\tau^2/K_r - 4\pi R_0 f_0/c \cdot \left[D(f_\eta) + \frac{f_\tau}{f_0 D(f_\eta)} + \frac{D^2(f_\eta)-1}{2f_0^2 D^3(f_\eta)} f_\tau^2\right] - \frac{4\pi R_0 f_0}{c} \cdot \sum_{i=3}^{n} \frac{\Upsilon_i}{i!} f_\tau^i$
5. $e^{j\Phi_{SS}} \times e^{j \cdot H_{HOPF}}$	$H_{HOPF} = \pi \cdot \sum_{i=3}^{n} X_i f_\tau^i$
6. Range IFFT $\rightarrow e^{j\Phi_{sSm}}$	$\Phi_{sSm} = \frac{-4\pi R_0 D(f_\eta) f_0}{c} + \pi K_m (\tau - \tau_d)^2 + \sum_{i=3}^{n} \left(\frac{4\pi R_0 f_0}{c}\frac{\Upsilon_i}{i!} - \pi X_i\right) K_m^i (\tau - \tau_d)^i$
7. $e^{j\Phi_{sSm}} \times e^{jH_{CS}}$	$H_{CS} = \pi q_2 \left(\tau - \tau_{ref}\right)^2 + \pi \sum_{i=3}^{n} q_i \left(\tau - \tau_{ref}\right)^i$
8. Rearange Terms $\rightarrow e^{j\Phi_{sSz}}$	$\Phi_{sSz} = \frac{-4\pi R_0 D(f_\eta) f_0}{c} + \sum_{i=0}^{n} C_i (\tau - \tau_s)^i$ $= \frac{-4\pi R_0 D(f_\eta) f_0}{c} + \pi\left(q_2 + K_f\right)(\tau - \tau_s)^2 + \pi \sum_{i=3}^{n} \left(q_i - X_i K_f^i + \frac{4f_0 \Upsilon_i R_{ref} K_f^i}{i!c}\right)(\tau - \tau_s)^i$ $+\pi K_m \Delta\tau^2 (\alpha - 1)^2 + \sum_{i=3}^{n} \left(\frac{2\pi K_m^i f_0 \Delta\tau^i \Upsilon_i (\Delta\tau c + 2R_{ref})}{i!c} - \pi K_m^i \Delta\tau^i X_i\right) + \sum_{i=2}^{n} \pi\alpha^i \Delta\tau^i q_i$
9. Range FFT $\rightarrow e^{j\Phi_{SS2}}$	$\Phi_{SS2} = \frac{-4\pi R_0 D(f_\eta) f_0}{c} - \left(\frac{4\pi R_{ref}(1-\alpha)}{cD(f_\eta)} + \frac{4\pi\alpha R_0}{cD(f_\eta)}\right) f_\tau - \frac{\pi\alpha f_\tau^2}{K_f} - \pi \sum_{i=3}^{n} \left(q_i - X_i K_f^i + \frac{4f_0 \Upsilon_i R_{ref} K_f^i}{i!c}\right) f_\tau^i$ $+\pi K_m \Delta\tau^2 (\alpha - 1)^2 + \sum_{i=3}^{n} \left(\frac{2\pi K_m^i f_0 \Delta\tau^i \Upsilon_i (\Delta\tau c + 2R_{ref})}{i!c} - \pi K_m^i \Delta\tau^i X_i\right) + \sum_{i=2}^{n} \pi\alpha^i \Delta\tau^i q_i$
10. $e^{j\Phi_{SS2}} \times e^{jH_R}$	$H_R = \frac{4\pi R_{ref} f_\tau (1-\alpha)}{cD(f_\eta)} + \frac{\pi\alpha f_\tau^2}{K_f} + \pi \sum_{i=3}^{n} \left(q_i - X_i K_f^i + \frac{4f_0 \Upsilon_i R_{ref} K_f^i}{i!c}\right) f_\tau^i$
11. Range IFFT $\rightarrow e^{j\Phi_{sSaz}}$	$\Phi_{sSaz} = \frac{-4\pi R_0 D(f_\eta) f_0}{c}$ $+\pi K_m \Delta\tau^2 (\alpha - 1)^2 + \sum_{i=3}^{n} \left(\frac{2\pi K_m^i f_0 \Delta\tau^i \Upsilon_i (\Delta\tau c + 2R_{ref})}{i!c} - \pi K_m^i \Delta\tau^i X_i\right) + \sum_{i=2}^{n} \pi\alpha^i \Delta\tau^i q_i$
12. $e^{j\Phi_{sSaz}} \times e^{jH_{az}}$	$H_{az} = \frac{4\pi R_0 D(f_\eta) f_0}{c}$ $-\pi K_m \Delta\tau^2 (\alpha - 1)^2 - \sum_{i=3}^{n} \left(\frac{2\pi K_m^i f_0 \Delta\tau^i \Upsilon_i (\Delta\tau c + 2R_{ref})}{i!c} - \pi K_m^i \Delta\tau^i X_i\right) - \sum_{i=2}^{n} \pi\alpha^i \Delta\tau^i q_i$
13. Azimuth IFFT	

the algorithm simplifies to the extended CSA of [15]. Also, when $n = 4$ it simplifies to the QPA [16] with a note that our algorithm includes a 4th order signal model. The extended CSA, non-linear CSA and QPA were all specifically developed for squint mode processing, but it is not only squinting that can cause the low-order approximations to break down. The approximation error has been dealt with more generally in this paper, but the method developed is well suited for squint-mode processing.

An approximation to the generalized algorithm that eliminates the extra range FFT and IFFT is obtained by, in Table III, eliminating rows 3-6 and combining row 5 with row 10. An example is shown in Fig. 15, where it is plain to see that the focusing is similar, but the sidelobes are larger.

V. CONCLUSION

With new SAR systems pushing center frequencies lower, bandwidths larger, and beamwidths wider, the approximations used in common frequency-domain SAR processing algorithms are inadequate. By developing an expression for the phase error term and visualizing it over the two-dimensional frequency support band, analysis of the effects of varying the SAR parameters for a given approximation is enhanced. RDA and CSA are low-order approximations of ideal frequency domain processing. A generalized algorithm is herein developed. A set of guidelines is proposed to determine the required approximation order for proper image processing, for a given set of SAR parameters. An efficient frequency-domain algorithm, built upon the CSA framework, which accounts for higher order terms is used to increase the precision over existing algorithms. Together, these tools provide an attractive alternative to the ω-k and time-domain methods for processing wide-beamwidth, low-frequency, large-bandwidth SAR data.

APPENDIX A
DERIVATION OF GENERAL SAR SIGNAL IN THE WAVENUMBER DOMAIN

For completeness, a summary of the derivation of the SAR signal in the wavenumber domain that is presented by Cumming and Wong in [31] is included in this appendix. The derivation consists of taking the range and azimuth Fourier transforms of Eq. (1). We approximate the Fourier transforms using the principle of stationary phase (POSP), which is valid except in the extreme case of having radar frequencies very close to zero.

An expression for the signal phase after the range Fourier transform is computed by adding the phase term $-2\pi f_\tau \tau$ to

TABLE IV
SOLVED HIGH-ORDER FILTER PARAMETERS AND CHIRP-SCALING TERMS

Parameter	Solution
q_2	$K_f \frac{1-\alpha}{\alpha}$
q_3	$K_s K_f^2 \frac{1-\alpha}{3\alpha}$
X_3	$\frac{-(\alpha-2)K_s c+(\alpha-1)2f_0\Upsilon_3 R_{ref}K_f}{3K_f c(\alpha-1)}$
q_4	$K_f^3 \frac{(\alpha-1)\left(f_0 D(f_\eta)c\Upsilon_3+6f_0 R_{ref}K_s K_f\Upsilon_3-9K_s K_f cX_3\right)+2K_s^2 c}{-12c\alpha}$
X_4	$\frac{(\alpha-2)\left(f_0 D(f_\eta)c\Upsilon_3+6f_0 R_{ref}K_s K_f\Upsilon_3-9K_s K_f cX_3\right)-(\alpha-1)2f_0\Upsilon_4 R_{ref}K_f+2K_s^2 c}{-12K_f c(\alpha-1)}$
q_5	$K_f^4 \frac{(\alpha-1)\left(f_0\Upsilon_4 D(f_\eta)c+8f_0\Upsilon_4 R_{ref}K_s K_f-48X_4 K_s K_f c\right)+6f_0 K_s\Upsilon_3\left(4R_{ref}K_f K_s+cD(f_\eta)\right)-36X_3 K_s^2 K_f c}{-60c\alpha}$
X_5	$\frac{(\alpha-2)\left(f_0 D(f_\eta)c\Upsilon_4+8f_0 R_{ref}K_s K_f\Upsilon_4-48K_s K_f cX_4\right)-(\alpha-1)2K_f f_0\Upsilon_5 R_{ref}+6f_0 K_s\Upsilon_3\left(4R_{ref}K_f K_s+cD(f_\eta)\right)-36K_s^2 K_f X_3}{-60K_f c(\alpha-1)}$
q_6	$K_f^5 \frac{8f_0 K_s\Upsilon_4\left(5R_{ref}K_s K_f+cD(f_\eta)\right)-(\alpha-1)\left(-f_0 D(f_\eta)c\Upsilon_5+300K_s K_f cX_5-10f_0 R_{ref}K_s K_f\Upsilon_5\right)-240K_s^2 K_f cX_4}{-360c\alpha}$
X_6	$\frac{(\alpha-2)\left(-300K_s K_f cX_5+f_0 D(f_\eta)c\Upsilon_5+10f_0 R_{ref}K_s K_f\Upsilon_5\right)-(\alpha-1)2f_0 R_{ref}K_f\Upsilon_6+8f_0\Upsilon_4 K_s\left(5R_{ref}K_s K_f+cD(f_\eta)\right)-240X_4 K_s^2 K_f c}{-360K_f c(\alpha-1)}$

Eq. (1), where f_τ is range frequency:

$$\Phi_{0r} = \frac{-4\pi f_0 R(\eta)}{c} + \pi K_r \left[\tau - \frac{2R(\eta)}{c}\right]^2 - 2\pi f_\tau \tau. \quad (25)$$

Take the derivative of the phase with respect to τ, and solve for τ at the point where the phase is stationary (i.e. where $d\Phi_{0r}/d\tau = 0$).

$$\frac{d\Phi_{0r}}{d\tau} = 2\pi K_r \left[\tau - \frac{2R(\eta)}{c}\right] - 2\pi f_\tau = 0 \quad (26)$$

$$\tau = \frac{f_\tau}{K_r} + \frac{2R(\eta)}{c}. \quad (27)$$

Substitute into Eq. (25) and simplify to obtain the signal phase after the range Fourier transform of the signal.

$$\begin{aligned}\Phi_{1R} &= \frac{-4\pi f_0 R(\eta)}{c} + \frac{\pi f_\tau^2}{K_r} - 2\pi f_\tau\left(\frac{2R(\eta)}{c} + \frac{f_\tau}{K_r}\right)\\ &= \frac{-4\pi f_0 R(\eta)}{c} - \frac{\pi f_\tau^2}{K_r} + \frac{-4\pi f_\tau R(\eta)}{c}\\ &= \frac{-4\pi(f_0+f_\tau)R(\eta)}{c} - \frac{\pi f_\tau^2}{K_r} \quad (28)\end{aligned}$$

We now expand the range to the target $R(\eta)$

$$R(\eta) = \sqrt{R_0^2 + v^2\eta^2} \quad (29)$$

where R_0 is the range of closest approach, and v is the velocity.

$$\Phi_{1R} = \frac{-4\pi(f_0+f_\tau)\sqrt{R_0^2+v^2\eta^2}}{c} - \frac{\pi f_\tau^2}{K_r}. \quad (30)$$

In order to evaluate the phase signal after the azimuth Fourier transform, again the POSP is used. Building the azimuth Fourier transform adds the term $-2\pi f_\eta \eta$ to the signal phase. Then the first derivative with respect to η is set to zero and solved for η.

$$\Phi_{1Ra} = \frac{-4\pi(f_0+f_\tau)\sqrt{R_0^2+v^2\eta^2}}{c} - \frac{\pi f_\tau^2}{K_r} - 2\pi f_\eta \eta \quad (31)$$

$$\frac{d\Phi_{1Ra}}{d\eta} = \frac{-4\pi f_0 v^2\eta}{c\sqrt{R_0^2+v^2\eta^2}} + \frac{-4\pi f_\tau v^2\eta}{c\sqrt{R_0^2+v^2\eta^2}} - 2\pi f_\eta = 0 \quad (32)$$

$$\begin{aligned}\eta &= -\frac{cf_\eta R_0}{v\sqrt{-f_\eta^2c^2+4v^2f_0^2+8v^2f_0f_\tau+4v^2f_\tau^2}}\\ &= -\frac{cf_\eta R_0}{2(f_0+f_\tau)v^2\sqrt{1-\frac{c^2f_\eta^2}{4v^2(f_0+f_\tau)^2}}} \quad (33)\end{aligned}$$

Substitute this into Eq. (31) and simplify with some algebraic manipulation to get the phase of the SAR signal in the wavenumber domain.

$$\begin{aligned}\Phi_{1RA} &= -\frac{4\pi(f_0+f_\tau)\sqrt{R_0^2+\frac{v^2c^2R_0^2f_\eta^2}{(f_0+f_\tau)^2v^4\left(4-\frac{f_\eta^2c^2}{v^2(f_0+f_\tau)^2}\right)}}}{c}\\ &+ \frac{\pi cR_0f_\eta^2}{(f_0+f_\tau)v^2\sqrt{1-\frac{c^2f_\eta^2}{4v^2(f_0+f_\tau)^2}}} - \frac{\pi f_\tau^2}{K_r}\\ &= -\frac{4\pi R_0(f_0+f_\tau)}{c\sqrt{1-\frac{c^2f_\eta^2}{4v^2(f_0+f_\tau)^2}}}\\ &+ \frac{\pi cR_0f_\eta^2}{(f_0+f_\tau)v^2\sqrt{1-\frac{c^2f_\eta^2}{4v^2(f_0+f_\tau)^2}}} - \frac{\pi f_\tau^2}{K_r}\\ &= -\frac{4\pi R_0(f_0+f_\tau)}{c}\sqrt{1-\frac{c^2f_\eta^2}{4v^2(f_0+f_\tau)^2}} - \frac{\pi f_\tau^2}{K_r}\\ &= -\frac{4\pi R_0f_0}{c}\sqrt{D^2(f_\eta)+\frac{2f_\tau}{f_0}+\frac{f_\tau^2}{f_0^2}} - \frac{\pi f_\tau^2}{K_r} \quad (34)\end{aligned}$$

where

$$D(f_\eta) = \sqrt{1-\frac{c^2f_\eta^2}{4v^2f_0^2}}, \quad (35)$$

and f_η is azimuth frequency.

REFERENCES

[1] S. Redadaa, J.M. Le Caillec, B. Solaiman, and M. Benslama, "Focusing problems of subsurface imaging by a low-frequency SAR," in *Proc. Int. Geosci. Rem. Sen. Symp.*, pp.4101-4104, July 2007.

[2] L.M.H. Ulander, M. Blom, B. Flood, P. Follo, P.0. Frolind, A. Gustavsson, T. Jonsson, B. Larsson, D. Murdin, M. Pettersson, U. Raaf, and G. Stenstrom, "Development of the ultra-wideband LORA SAR operating in the VHF/UHF-band," in *Proc. Int. Geosci. Rem. Sen. Symp.*, vol.7, pp. 4268-4270, July 2003.

[3] M.A. Ressler, "The Army Research Laboratory ultra wideband Boom-SAR," in *Proc. Int. Geosci. Rem. Sen. Symp.*, vol.3, pp.1886-1888, May 1996.

[4] H. Hellsten, "CARABAS-an UWB low frequency SAR," in *IEEE MTT-S Int. Microwave Symposium Digest*, vol.3, pp.1495-1498, June 1992.

[5] H. Nguyen, H. Roussel, and W. Tabbara, "A coherent model of forest scattering and SAR imaging in the VHF and UHF-band," in *IEEE Trans. Geoscience and Remote Sensing*, vol.44, no.4, pp. 838-848, April 2006.

[6] G. Smith-Jonforsen, L.H.H. Ulander, and Xianyun Luo, "Low VHF-band backscatter from coniferous forests on sloping terrain," in *IEEE Trans. Geoscience and Remote Sensing*, vol.43, no.10, pp. 2246-2260, Oct. 2005.

[7] A.T. Manninen, and L.M.H. Ulander, "Forestry parameter retrieval from texture in CARABAS VHF-band SAR images," in *IEEE Trans Geoscience and Remote Sensing*, vol.39, no.12, pp.2622-2633, Dec 2001.

[8] L.M.H. Ulander, and P.O. Frolind, "Ultra-wideband SAR interferometry," in *IEEE Trans. Geoscience and Remote Sensing*, vol.36, no.5, pp.1540-1550, Sept 1998.

[9] H. Israelsson, L.M.H. Ulander, J.L.H. Askne, J.E.S. Fransson, P.O. Frolind, A. Gustavsson, and H. Hellsten, "Retrieval of forest stem volume using VHF SAR," in *IEEE Trans. Geoscience and Remote Sensing*, vol.35, no.1, pp.36-40, Jan 1997.

[10] L.M.H. Ulander, and P.O. Frolund, "Ultra-wideband and low-frequency SAR interferometry," in *Proc. Int. Geosci. Rem. Sen. Symp.*, vol.1, pp.668-670, May 1996.

[11] J.M. Swiger, "Resolution limits of ultra wideband synthetic aperture radar using a rectangular aperture for FFT processing," *IEEE Trans. Aerospace and Electronic Systems*, vol.30, no.3, pp.935-938, Jul 1994.

[12] R. Goodman, S. Tummala,and W. Carrara, "Issues in ultra-wideband, widebeam SAR image formation," in *Record of the IEEE 1995 Int. Radar Conf.*, pp.479-485, May 1995.

[13] A. Moreira and Y. Huang, "Airbome SAR Processing of Highly Squinted Data Using a Chirp Scaling Approach with Integrated Motion Compensation," in *IEEE Trans. Geoscience and Remote Sensing*, vol.32, no.5, pp. 1029-1040, Sept. 1994.

[14] G.W. Davidson, I.G. Cumming, and M.R. Ito, "A Chirp Scaling Aproach for Processing Squint Mode SAR Data," in *IEEE Trans. on Aerospace and Electronic Systems*, 32 (1), pp. 121-133, Jan. 1996.

[15] A. Moreira, J. Mittermayer, and R. Scheiber, "Extended Chirp Scaling Algorithm for Air- and Spaceborne SAR Data Processing in Stripmap and ScanSAR Imaging Modes," in *IEEE Trans. Geoscience and Remote Sensing*, vol.34, no.5, pp. 1123-1136, Sept. 1996.

[16] K. Wang and X. Liu, "Quartic-Phase Algorithm for Highly Squinted SAR Data Processing," in *IEEE Geoscience and Remote Sensing Letters*, vol.4, no.2, pp.246-250, April 2007.

[17] R. Rau, and J.H. McClellan, "Analytic models and postprocessing techniques for UWB SAR," in *IEEE Trans. Aerospace and Electronic Systems*, vol.36, no.4, pp. 1058-1074, Oct 2000.

[18] A. Potsis, A. Reigber, J. Mittermayer, A. Moreira,and N. Uzunoglou, "Improving the focusing properties of SAR processors for wide-band and wide-beam low frequency imaging," in *Proc. Int. Geosci. Rem. Sen. Symp.*, pp.3047-3049, vol.7, 2001.

[19] G. Fornaro, G. Franceschetti, and S. Perna, "On center-beam approximation in SAR motion compensation," in *IEEE Geoscience and Remote Sensing Letters*, vol.3, no.2, pp. 276-280, April 2006.

[20] A. Potsis, A. Reigber, E. Alivizatos, A. Moreira, and N.K Uzunoglou. "Comparison of Chirp Scaling and Wavenumber Domain Algorithms for Airborne Low-Frequency SAR." In *Francesco Posa, editor, SAR Image Analysis, Modeling, and Techniques V*, vol 4883, pp. 25-36, March 2002.

[21] H. Hellsten and L.E. Andersson, "An inverse method for the processing of synthetic aperture radar data," in *Inverse Problems* vol.3, pp. 111-124, 1987.

[22] A. Reigber, E. Alivizatos, A. Potsis, and A. Moreira. "Extended wavenumber-domain synthetic aperture radar focusing with integrated motion compensation." in *Proc. IEEE Radar, Sonar nd Navigation*, Vol. 153, Iss. 3, pp.301-310, June 2006.

[23] M.C. Cobb, and J.H. McClellan, "Omega-k quadtree UWB SAR focusing," in *Proc. IEEE Radar Conference*, pp.311-314, 2001.

[24] G. Choi, and D.C. Munson, "On the optimality and exactness of wavenumber-domain SAR data processing," in *Proc. Int. Conf. Image Processing*, vol.1, no., pp.456-460 vol.1, 13-16 Nov 1994.

[25] T.K. Sjogren, V.T. Vu, and M.I. Pettersson, "A comparative study of the polar version with the subimage version of Fast Factorized Backprojection in UWB SAR," in *2008 Int. Radar Symposium*, pp.1-4, May 2008.

[26] L.M.H. Ulander, H. Hellsten, and G. Stenstrom, "Synthetic-aperture radar processing using fast factorized back-projection," in *IEEE Trans. Aerospace and Electronic Systems*, vol.39, no.3, pp. 760-776, July 2003.

[27] A.F. Yegulalp,"Fast backprojection algorithm for synthetic aperture radar," in *The Record of the 1999 IEEE Radar Conference*, pp.60-65, 1999.

[28] M. Blom and P. Follo, "VHF SAR image formation implemented on a GPU," in *Proc. Int. Geosci. Rem. Sen. Symp.*, vol.5, pp. 3352-3356, 2005.

[29] S.N. Madsen, "Motion compensation for ultra wide band SAR," in *Proc. Int. Geosci. Rem. Sen. Symp.*, vol.3, pp.1436-1438, 2001.

[30] A. Reigber, A. Potsis, E. Alivizatos, N. Uzunoglu, and A. Moreira, "Wavenumber domain SAR focusing with integrated motion compensation," in *Proc. Int. Geosci. Rem. Sen. Symp.*, vol.3, pp. 1465-1467, July 2003.

[31] I.G. Cumming and F.H. Wong, *Digital Processing of Synthetic Aperture Radar Data*, Artech House, 2005.

[32] R.K. Raney, H. Runge, R. Bamler, I.G. Cumming, and F.H. Wong, "Precision SAR processing using chirp scaling," in *IEEE Trans. Geoscience and Remote Sensing*, vol.32, no.4, pp.786-799, Jul 1994.

[33] L. Jin and X. Liu, "Nonlinear Frequency Scaling Algorithm for Squint Spotlight SAR Data Processing," in *EURASIP Journal on Advances in Signal Processing*, vol. 2008, Article ID 657081, 8 pages, 2008.